Pickering emulsions stabilized with differently charged particles

Mathis Benyaya, Marie-Alexandrine Bolzinger, Yves Chevalier, Salomé Ensenat, Claire Bordes

ARTICLE

Pickering emulsions stabilized with Differently Charged Particles

Mathis Benyaya*, Marie-Alexandrine Bolzinger, Yves Chevalier, Salomé Ensenat, Claire Bordes*

Received 00th January 20xx,
Accepted 00th January 20xx

DOI: 10.1039/x0xx00000x

For addressing health issues and ecological concerns, the cosmetic and pharmaceutical industries are facing the challenge of designing emulsions without the use of surfactants. Emulsions stabilized by colloidal particles, known as Pickering emulsions, are promising to that matter. In this article, three different types of particles (neutral, anionic and cationic) were used alone or in binary mixtures as stabilizers of Pickering emulsions. The influence of the particles' charge on the emulsions' properties and the synergies between the different types of particles were studied. It is demonstrated that the kinetics of adsorption of the particles at the water/oil interface control the coverage and their organization at the droplets surface, rather than their interactions after adsorption. Binary mixtures of differently charged particles are a powerful way to control the droplet coverage and the particle loading in the emulsions. In particular, the combination of anionic and cationic particles led to smaller droplets and higher particles coverage of emulsion droplets.

Abbreviations

A-PMMA: Anionic PMMA-like copolymer, similar abbreviation was used for neutral (N-PMMA) and cationic (C-PMMA) copolymers.
a-PMMA: Particles obtained from A-PMMA copolymer, similar abbreviation was used for n- and c-pmma particles.
A-emulsion: Emulsion made from a-PMMA, similar abbreviation was used for N- and C-emulsions.
A/C-emulsion: Emulsion made with mixed anionic and cationic particles, similar abbreviation was used for A/N- and N/C-emulsions. If no precision is given, the mixing is 50/50 w/w.
MTPs: Mono-Type Particles emulsions, refers to A-, N- and C-emulsions.
DCPs: Differently Charged Particles emulsions, refers to A/C-, A/N, and N/C-emulsions.
OCPs: Oppositely Charged Particles emulsions, refers to A/C-emulsions.
MSD: Minimum size of the droplets
MSD_d: Dimensionless MSD

1. Introduction

Emulsions are very common in cosmetic, pharmaceutical or food products. Pickering emulsions are emulsions stabilized by colloidal particles in place of surfactants adsorbed at the water/oil interface. Pickering emulsions have shown very interesting properties such as a great stability against coalescence (1–3), or unique drug delivery kinetics (4,5). Indeed, Simovic *et al.* demonstrated that Pickering emulsions induce a better skin retention of drugs than classical emulsions. Frelichowska *et al.* (4) showed that the topical delivery flux of caffeine was higher using Pickering emulsions compared to classical (surfactant-based) ones. Moreover, avoiding the use of surfactants is interesting as they can be irritating and environmentally concerning. This is why many researches were devoted to the potential pharmaceutical applications of such system (6). The number of patents claiming Pickering emulsions for the pharmaceutical and cosmetic fields highly increased during the last years. According to Espacenet, the number of patents applications was about 20 in 2000, about 100 in 2005 and reached around 500 per year since 2018. However, Pickering emulsions in current industrial products are most of the time ignored, and simply qualified as emulsions by lack of characterization; a typical example is sunscreen creams (7). But Pickering emulsions were also investigated in many other industrial fields, as the ceramic production for example (8,9). The main limitation to the development of Pickering emulsions as industrial products is the lack of scientific background, which makes the prediction and control of their properties difficult, especially when several types of particles are mixed as stabilizers.

Pickering emulsions may be obtained using several different types of colloids as emulsifiers. The colloids can vary in nature, size, or shape. For example, Oppositely Charged Particles (OCP) emulsions are Pickering emulsions stabilized by both anionic and cationic particles. There are relatively few studies dedicated to OCP emulsions (9–14). Zembyla *et al*. (12) demonstrated a synergistic effect between anionic and cationic particles that could both stabilize the emulsion and create a particle network that favored the emulsion stability by increasing the continuous phase viscosity. OCPs were also claimed to assemble in an adsorbed double layer, thus increasing the stability of the emulsions. Zhang *et al.* (14) used positively charged pea protein microgels (PPM) and negatively charged cellulose nanocrystals

Authors from : Université de Lyon, Université Claude Bernard Lyon 1, CNRS UMR 5007, Laboratoire d'Automatique, de Génie des Procédés et de Génie Pharmaceutique (LAGEPP), 43 bd du 11 Novembre 1918, 6962, Villeurbanne, France.
**: corresponding authors*
Electronic Supplementary Information (ESI) available: [details of any supplementary information available should be included here]. See DOI: 10.1039/x0xx00000x

(CNC) to study a potential gastric delivery system. The PPM-based emulsions were destabilized at low pH. The addition of CNC allowed the formation of a stabilizing double layer of mixed particles that limited the coalescence in the gastric medium. Finally, Nallamilli *et al.* (10) proposed a model to predict the size of the droplets for OCPs made with latex particles. They studied the case where only the particles present in an aggregate could adsorb at the droplets surface. The impact of the use of mixed charged and neutral particles is poorly documented. The study of this type of emulsions can offer both a better understanding of Pickering emulsion formation mechanism and a new way to design emulsion with controllable properties, two requirements for the development of Pickering emulsions-based products.

In this article, Pickering emulsions were prepared using two types of differently charged polymeric particles as stabilizers. The objective was to investigate the influence of the particle mixture composition on the coverage of the emulsion droplets by the particles and on the droplet size. Indeed, the control of these parameters is of main relevance to control the emulsion stability, its rheological properties and its potential use as drug delivery system (15–18).

For this purpose, three types of polymeric particles with different surface charges were formulated from one neutral, one anionic and one cationic copolymers. To only study the impact of their surface charges on the emulsion properties, the used copolymers were synthesized with methyl methacrylate (MMA)-derivatives comonomers so as to be as close in chemical structure. Thus, the obtained polymers were derived from poly(methyl methacrylate) (PMMA) which is a well-known biocompatible and non-biodegradable polymer. PMMA is largely used in prosthesis medical field for dental implant or bone reconstruction (19).

Pickering emulsions made of a cosmetic oil were then prepared with each type of particle or by using a combination of two types of particles. The droplet size and the particles organization at the surface of the droplets were studied and discussed in relation with the emulsion composition and process of emulsification. The impact of the effective charges of the particles on the emulsion properties was especially investigated, and the importance of particle adsorption kinetics was demonstrated.

2. Materials and methods

2.1. Raw materials

Methyl methacrylate (purity ≥ 99.0%) (MMA) from Sigma-Aldrich, methacrylic acid (purity ≥ 99.5%) (MAA) from Acros Organics, hydroxyethyl methacrylate from Sigma-Aldrich (HEMA), and 2-(dimethylamino)ethyl methacrylate from Sigma-Aldrich (DMAEMA) were used as monomers to synthetize the copolymers used for the formulation of the particles. The different solvents used during these syntheses were tetrahydrofuran (purity ≥ 99.0%) purchased from Sigma-Aldrich and heptane (purity ≥ 99.0%) from VWR chemicals. 2,2′-Azobis(2-methylpropionitrile) (AIBN) from Sigma-Aldrich was used as an initiator of the reaction. Ethyl acetate (purity ≥ 99.5%) from Sigma was used for the formulation of the particles as the organic phase. The fluorophores encapsulated were Nile red purchased from TCI and ATTO 425 NHS-Ester purchased from Atto-tec. Mowiol 4-88 purchased by Sigma-Aldrich was the poly(vinyl alcohol) (PVA) used as the emulsifier for the particles preparation. A classical oil used in cosmetic products was chosen: isononyl isononanoate was supplied by Stéarinerie Dubois.

2.2. Polymers synthesis and characterization

2.2.1. Polymers synthesis. Many MMA-derivative monomers polymerize in the same way and can undergo random copolymerization. Methacrylic acid (MAA), hydroxyethyl methacrylate (HEMA) or 2-(dimethylamino)ethyl methacrylate (DMAEMA) were used as comonomers of MMA to synthetize anionic, neutral and cationic "PMMA-like" copolymers. Several syntheses using combinations of these monomers have already been reported in the literature (20–23). PMMA was chosen as a main polymer because it is biocompatible. Indeed, no report concerning its toxicity for pharmaceutical use was found. In this study, the diameter of the particles was wanted to be around 1 µm, for being observable with a confocal microscope and being suited for cosmetic or pharmaceutical applications.

The synthesis of PMMA-like copolymers was done using a simple free-radical polymerization process (24). Anionic PMMA (A-PMMA) was obtained by combining MMA and MAA monomers at 95/5 weight ratio. Neutral PMMA (N-PMMA) was obtained by combining MMA and HEMA monomers at 95/5 weight ratio. Cationic PMMA (C-PMMA) was obtained by combining MMA and DMAEMA monomers at 90/10 weight ratio. This latter ratio was chosen differently in order to obtain enough charges at the surface of the final particles. Polymerization in tetrahydrofuran (THF) solution was performed at 60 °C in a reflux flask system under nitrogen flow to prevent any deactivation of radicals by oxygen. The polymerization recipe contained 15 g of monomers in 300 mL THF. 0.3 g of AIBN initiator was added into the deoxygenated monomer solution at 60 °C for starting the free radical polymerization reaction. After 5 h, the mixture was left to cool down to room temperature, and a precipitation step was operated. The solution was poured dropwise into a large amount of heptane under vigorous stirring. Heptane was chosen as the precipitation solvent as it is miscible with THF while being a non-solvent for PMMA making the polymer precipitation possible (25). The suspension was filtered on sinter-glass filter, rinsed with water, and the powder was vacuum-dried at 105 °C for 24 h. The temperature was higher than heptane and THF boiling points (96 °C and 80 °C, respectively), but lower than the degradation temperature of PMMA (about 175 °C). The polymer was regularly crushed using a mortar with pestle during the drying period.

2.2.2. Polymers characterizations. ^{1}H NMR spectra were recorded on a Bruker AVL300 at the CCRMN of Lyon 1 University

(https://ccrmn.univ-lyon1.fr/). Solvent used was deuterated chloroform.

Differential Scanning Calorimetry (DSC) analyses were performed to determine the glass transition temperature of the three synthetized polymers. The measurements were performed with a DSC Q200 (TA Instruments, New Castle, DE). Samples were put into sealed aluminum crucibles and submitted to two cycles of heating and cooling. The presented results are those of the second heating cycle performed between 20 °C and 120 °C (or 150 °C) with a heating rate of 10 °C·min^{-1}.

2.3. Particles formulation and characterization

2.3.1. Particles formulation. PMMA-like particles were obtained by the emulsion/solvent evaporation method (24). 1.25 g of polymer were dissolved in 10 mL of ethyl acetate possibly together with a small amount of fluorescent dye (a grain of fluorophore powder). Cationic particles were marked by Nile red. Anionic particles were marked by coumarin. Neutral particles were marked by one of the two fluorophores depending on the experiment. 15 mL of an aqueous solution of 0.8 wt% PVA were mixed with the organic solution by means of an UltraTurrax rotor-stator mixer at 24 000 rpm for 5 min. PVA concentration was chosen so as to obtain particles with a size of about 0.8 µm. The removal of excess PVA was checked by surface tension measurements (24).

The emulsion was then added into 150 mL of distilled water and left at least for 3 h under gentle stirring to allow the extraction/evaporation of ethyl acetate. The suspension was cleaned 7 times by centrifugation and renewal of the supernatant water to eliminate the PVA and the possible residual organic solvents. The particles were finally resuspended in 40 mL of water under vigorous stirring and submitted to ultrasounds to break possible aggregates.

For the charged particles, a tempering process as previously described in (24) was necessary for the surface charge to appear. The anionic (resp. cationic) particles were put in a water solution at pH = 13.5 (resp. pH = 0.7) for 10 min (resp. 5 min). Then, they were diluted ten times with distilled water. The suspension was centrifuged for 10 min at 6000 rpm and the supernatant water was thrown away and replaced by distilled water. This step was done 3 more times to obtain a suspension with a neutral pH.

For the rest of the article, a-PMMA will refer to “particles obtained from A-PMMA polymer”; and this is the same for cationic (c-PMMA) and neutral particles (n-PMMA).

2.3.2. Particles characterization. A cleaning step used to remove PVA from the particle suspensions has been precisely described in (24). The particle concentration in the obtained suspensions was determined by weighing the dry extract. For each suspension, measurements were performed in triplicate. The concentrations were close to 2 %w/w with a standard deviation of 0.1% for all of the particles type.

Particle size distributions were determined using a small-angle light scattering (Mastersizer 3000, Malvern Panalytical). The used real part of the refractive index was that of PMMA (1.49) and its imaginary part was zero for all the particles. Measurements were made in triplicate at a stirring rate of 1400 rpm. In Table 2 standard deviation is the standard deviation on the three measurements of the median diameter. Span represents the width of the distribution and is calculated as (D(90)-D(10))/D(50), with D(X) the diameter for which X% of the particles are smaller.

ζ-potentials were measured at several pH using a Zetasizer instrument from Malvern Panalytical. Concentrated HCl or NaOH solutions were used to vary the pH. Prior to the measurements, the suspensions were diluted with water till a low enough conductivity (~1.3 mS·cm^{-1}) was reached because ζ-potential measurements at high ionic strengths are of poor accuracy.

Scanning electron microscopy pictures were taken using a Jeol Neoscope JCM5000 to verify the sphericity of the particles.

The particles were made fluorescent by the use of two different fluorophores. The maximum absorption wavelength of the coumarin ATTO 425 dye is 439 nm, for a maximum emission at 485 nm. For Nile Red, these values are respectively 552 nm and 636 nm. The use of these two fluorophores with well-separated emission spectra allowed the visualization of each type of particles in their mixture stabilizing the differently charged particles emulsions by using a Zeiss LSM 800 confocal fluorescence microscope.

2.4. Emulsions formulation and characterization

2.4.1. Emulsions formulation. The suspensions of polymer particles were diluted with water until obtaining 8 g of suspension. Emulsions were prepared by mixing 2 g of oil in the suspension with an UltraTurrax mixer at two different stirring rates and durations: at 24 000 rpm for 6 min or at 6 500 rpm for 20 min.

In the case of emulsions stabilized by differently charged particles using mixtures of two different types of particles, both suspensions were put together into the vial before adding supplementary water to reach the desired concentration. In the case of a-PMMA and c-PMMA mixtures, large aggregates quickly formed.

For the rest of the article, “emulsion made from a-PMMA” will be noted as A-emulsion. Same denomination will be used for C-emulsion and N-emulsion. These emulsions will also be referred to “mono-type particles emulsions” or MTPs.

A/C-emulsion designates an emulsion made with mixed anionic and cationic particles. If nothing else is specified, the mixture is made with 50/50 w/w of both particles. Same denomination will be used for A/N-emulsion and N/C-emulsion. These emulsions will also be referred to “differently-charged particles emulsions” or DCPs. In particular, A/C-emulsion will be referred to OCP, meaning “oppositely charged particles emulsion”.

2.4.2. Emulsions characterization. The droplet size was determined by analyzing optical microscopy images. The Image J software was used to measure the diameter of about 100 droplets, and the calculated median diameter was used as a measurement of the mean droplet size.

CLSFM (confocal laser scanning fluorescence microscopy) was used to observe the particles organization at the oil/water interface. A 3D representation of the emulsions was obtained by stacking different images taken along the *z*-axis using Image J. Some images were improved in terms of brightness or contrast and a fast Fourier transform filter was sometimes used to distinguish the different types of mixed particles.

3. Results and discussion

3.1. Physicochemical properties of the polymeric particles

3.1.1. Polymer characterization. ^{1}H NMR analyses confirmed that polymerization went to completion and that no residual monomer was present in the final products for A-PMMA, N-PMMA and C-PMMA copolymers. The two peaks characteristic of the C=C bond at 5.2 and 5.7 ppm disappeared and one peak appeared at 1.8 ppm assigned to a CH_2 group. The peak at 3.6 ppm is typical of the MMA ester function (Figure S1).

DSC measurements were performed to determine the glass transition temperature (T_g) of the synthesized polymers. The experimental results were compared to theoretical values obtained by using the comonomer *c* reported in the Polymer Handbook (26) and the Fox equation (27): $\frac{1}{T_g} = \sum\left(\frac{w_i}{T_{g_i}}\right)$, with T_g the glass transition temperature of the copolymer, w_i the mass ratio of each co-monomer in the mixing, and T_{g_i} the glass transition temperature of each pure polymer based on these monomers.

Differences lower than 15 °C were observed, thus confirming that the copolymers were successfully synthetized with very few contaminations detected (Table 1). They were then used to prepare particles using an o/w emulsion with solvent extraction/evaporation method as described in part 2.3.1.

3.1.2. Particles characterization

Particle size distribution. The amount of PVA was determined so as to obtain particles with size about 1 µm whatever the polymer used and to conserve a unique preparation protocol for all types of particles. As reported in Table 2, the three batches of particles exhibited a median diameter between 650 and 950 nm with a narrow distribution. From a Pickering emulsion stabilizer point of view, such particle sizes were considered as similar. Indeed, some studies showed that the diameters of emulsions droplets made with particles between 0.5 and 1 µm only varied by 20% (28,29). For the rest of the study, the diameters of the particles were thus considered as monodisperse with their size equal to their median diameter.

Particles shapes. All the particles were spherical, as shown in a previous work (24) (Figure S2).

PVA contamination. A cleaning procedure made of several water washing steps at the end of the particle preparation process was necessary to ensure that no PVA remained in the particle suspensions. PVA quantification by surface tension measurements indicated that 7 water washing steps allowed the removal of PVA from the suspensions (24).

Surface charges of the PMMA-like particles. Expectations were to have pH-dependent ζ-potential negative for the a-PMMA, around zero for the n-PMMA and positive for the c-PMMA. The charges were coming from ionization reactions of the carboxylic acid groups of a-PMMA or of the amine groups of c-PMMA. A tempering step was necessary to shift the charges to the particles surface. Before this latter step, no charges were detected by ζ-potential measurements for a-PMMA and c-PMMA (Figure 1). The mechanism of charge appearance was already described in a previous article (24).

All the emulsions were made at a neutral pH, around 7. The goal was to obtain particles with a ζ-potential higher in absolute value than 10 mV at neutral pH. As seen in Figure 1, at neutral pH, the a-PMMA and c-PMMA are charged after the tempering process, and n-PMMA is neutral. It is worth noting that for c-PMMA, it was necessary to synthetize a polymer with 10 wt% of comonomer to obtain enough surface charges, i.e. a ζ-potential ~20 mV. The charge of a cationic particles was calculated from the ζ-potential using the equation from Ohshima *et al.* (30) and was about twice more than that of anionic ones (ζ-potential ~−10 mV).

Fluorophore encapsulation. Polymer particles were loaded with fluorescent dyes for making possible the visualization of the particles organization at the surface of the emulsion droplets. Particles were labelled either by Nile red emitting fluorescence at 636 nm (n-PMMA and c-PMMA), or by coumarin emitting fluorescence at 485 nm (n-PMMA and a-PMMA). Evidence of successful encapsulation of fluorophores was given by CLSFM (Figure 2) showing the fluorescence emission of the fluorophores present in the particles, and no fluorescence background outside the particles.

Table 1. Theoretical and experimental values of the glass transition temperature for each copolymer.

	% of MMA (w/w)	% of comonomer (w/w)	T_g (°c) *Theoretical*	T_g (°c) *Measured*
A-PMMA	95.0%	5.0%	108	119
N-PMMA	95.0%	5.0%	103	92
C-PMMA	90.0%	10.0%	112	102

Table 2. Size characteristics of the three particles batches.

	Median diameter (µm)	Standard deviation (nm)	Span
a-PMMA	745	8	1.63
n-PMMA	644	6	1.14
c-PMMA	953	15	1.15

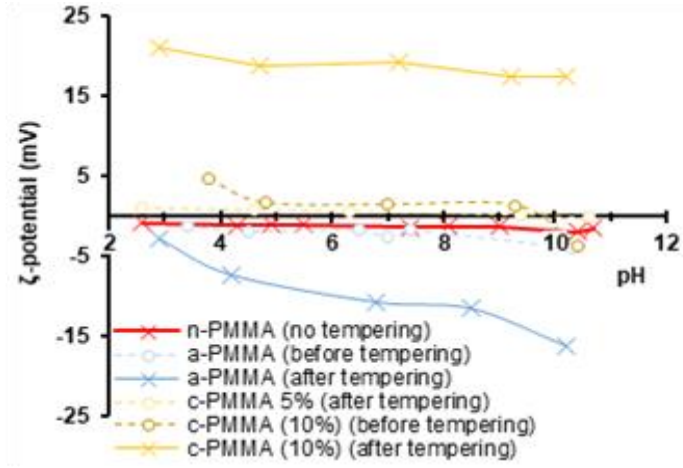

Figure 1. Experimental measurements of the ζ-potential before and after the tempering (if needed). The solid lines are the ones measured from the final particles used.

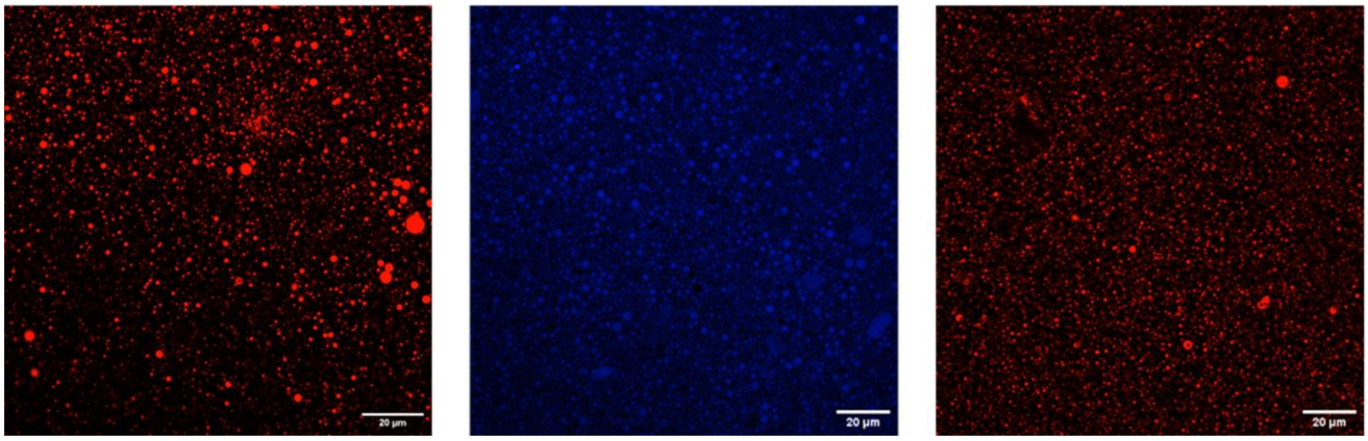

Figure 2. CLSFM pictures of the particles containing fluorophores. From left to right, n-PMMA (Nile red), a-PMMA (coumarin), c-PMMA (Nile red). n-PMMA were also prepared with coumarin but their pictures are not shown.

3.2. Pickering emulsions

3.2.1. Emulsions formulation and stability. The particles-to-oil ratio has been already shown as a determining parameter of the properties of Pickering emulsions (18). Emulsions were prepared with different mass of particles at a constant volume of oil. First, emulsions with a single type of particle were studied. Then, emulsions with two types of particles (a/n-, a/c- and n/c-pmma) were investigated in different proportions 25/75, 50/50 and 75/25 w/w. Whatever the operating conditions, creamed emulsions were obtained. Creaming occurred within a few seconds whatever the operating conditions. After about one hour, a slightly turbid aqueous layer phase was observed at the bottom of the emulsion. The stability of the emulsions was assessed by their visual aspect. The emulsions were considered as unstable when a layer of oil was observed on top of it.

The minimum concentration of particles required to obtain a stable emulsion was determined by preparing emulsions with a varying mass concentration of particles in oil from 2.1 to 6.4 mg·cm^{-3} and looking at any oil release on top of the emulsion. The minimum particle concentration in oil required for stabilizing the emulsions was about 6 mg·cm^{-3}, whatever the particles type used as stabilizer. Emulsions made with a smaller mass of particles did not allow the emulsification of the total volume of the oil introduced. As an example, Figure 3 presents emulsions obtained with concentrations of n-PMMA particles in oil ranging from 2.1 up to 6.4 mg·cm^{-3}; only the emulsion containing 6.4 mg·cm^{-3} of particles allowed the emulsification of the full oil content. Droplets sizes were quite large such that it could be visually seen that a diminution of the particles-to-oil ratio caused a noticeable increase of the droplets diameter in the part containing the fraction of emulsified oil. Similar results were obtained for all the emulsions. Other pictures of emulsions are presented in Figure S3. For the rest of the study, particle concentrations in oil were ranging from 8 up to 200 mg·cm^{-3}, far above from the minimum particle concentration required for ensuring the stability. The size of their droplets was measured from microscopy images as previously described. To estimate the standard deviation associated to these size measurements, five identical emulsions were prepared at three different concentrations in oil (8.0, 10.6, 21.2 mg·cm^{-3}) for each of the three single particle type emulsions. The standard deviations ranged between 7% and 10% of the emulsion median droplet size. A standard deviation about 9% of the emulsion droplet size was thus taken as the experimental error for the emulsion size measurements between 50 and 400 µm.

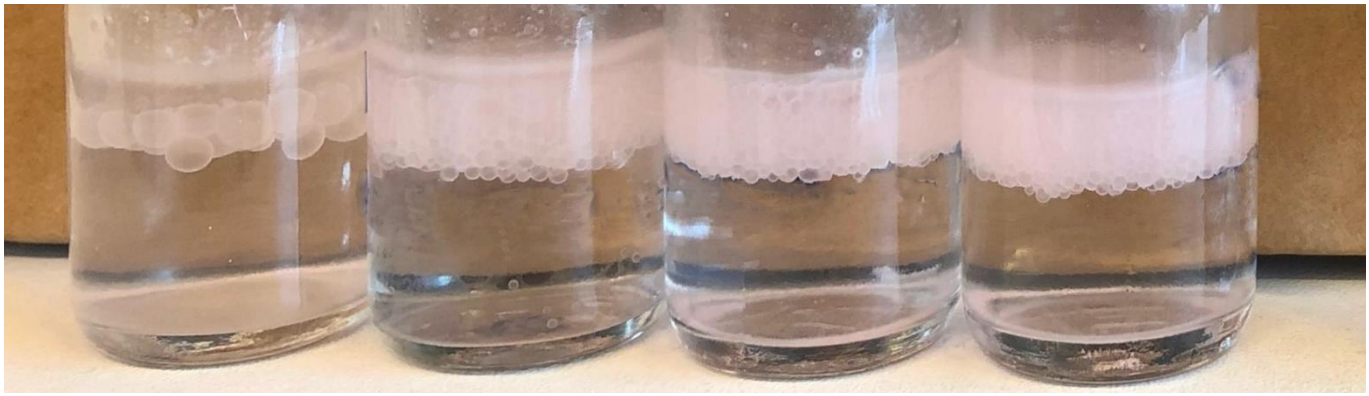

Figure 3. Emulsions made with n-PMMA as emulsifier at different particle concentrations of 2.1, 3.2, 4.3 and 6.4 mg of particles per cm³ of oil (left to right). The layer at the top of the emulsion corresponds to non-emulsified oil. Results were similar for other emulsions.

3.2.2. Median size and coverage of the emulsion droplets.

Particles coverage. The coverage of the droplet surface by the stabilizing particles was calculated using the following equation based from geometric considerations (31):

$$Coverage = \frac{d_d\, c_p}{4\, \rho\, d_p} \quad \text{(Eq. 1)}$$

with d_d the droplet diameter, c_p the concentration in particle defined as $\frac{mass\ of\ particles}{volume\ of\ oil}$, ρ the density of the polymer, d_p the diameter of a particle. For the DCP emulsions, d_p was taken as the mean diameter of the particles weighted by their mass fractions. A coverage of 100% means that the water/oil interface is fully covered by a monolayer of particles. If all particles are spherical, geometric considerations imply that the maximum coverage that can be reached is 91%, corresponding to a compact hexagonal organization as a monolayer.

In all cases, the full content of polymer particles adsorbed to oil droplets. A clear evidence was given by an analysis of the aqueous phase. Centrifugation of the emulsion yield a creamed layer of emulsion droplets and a clear subnatant. There was no sedimented polymer particles at the sample bottom. Drying the collected aqueous phase did not reveal any significant mass of free particles. The light scattering measurement of droplet size distribution also showed that there was no free polymer particles. If any, a supplementary population of size around 1 µm would have easily been observed as in the case of Pickering emulsions stabilized by excess silica particles (18).

At a constant volume of oil, the size of the droplets in Pickering emulsions decreased linearly with respect to the mass concentration of particles. Such linear behavior indicated that the coverage did not depend on the concentration of particles introduced (18). Indeed, a higher concentration of particles allows stabilizing a larger interfacial area between water and oil, and consequently smaller oil droplets. Accordingly, the coverage can be deduced from the slope of the plot of the droplet diameter as a function of the concentration of particles:

$$Coverage = \frac{slope}{4\, \rho\, d_p} \quad \text{(Eq. 2)}$$

During an emulsification process, two phenomena occur at the same time: i) the mixing device breaks the droplets, diminishing their size and some particles adsorb at the created interface to stabilize it and ii) some droplets merge by back-coalescence. The linear regime previously described corresponds to a case where the droplet size is controlled by the adsorption of the particles at the oil/water interface, which is the limiting phenomenon that sets the droplets size during the emulsification process. This has been described at the "limited coalescence process" (32). When the power of the mixing device (i.e. its ability to break up droplets) is not enough for fragmentation of droplets down to the size allowed by the concentration of particles, particles in excess remain in suspension in the continuous phase and the droplet size no longer depends on the concentration of particles. At this point, the minimum size of the droplets (MSD) is reached.

MTPs: Emulsions made with a single type of particle. The size of emulsions prepared with one single type of particle (a-, n- or c-PMMA) is presented in Figure 4 as a function of the inverse of the mass of particles for a constant oil volume. Results showed that for PMMA-like particles, the expected linearity was observed with a very good correlation (R^2 > 0.92) for particle concentrations in oil from 8 up to 40 mg cm^{-3} (corresponding to median diameters between 60 µm and 400 µm). The coverage of the droplets was determined for each of the single- particle type emulsions by using Equation 2 (Table 3).

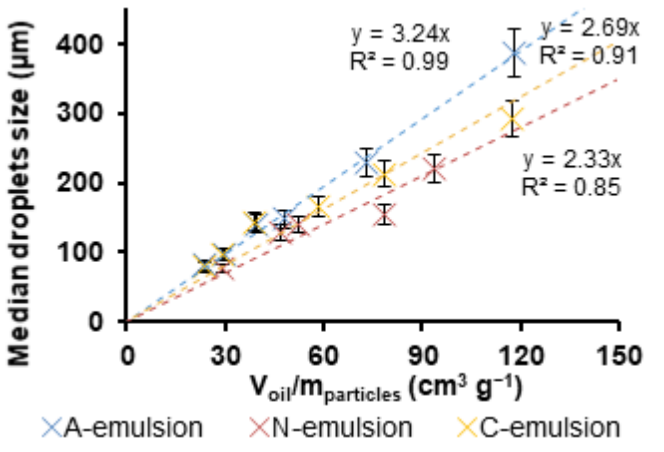

Figure 4. Median size of the droplets of the Pickering emulsions prepared with a single type of particles as a function of the inverse of the particle amount. The volume of oil was kept constant and the mass of particles varied.

Table 3. Coverages by particles of the different MTPs prepared at 24 000 rpm and at 6 500 rpm. They were calculated using the slopes of the regression lines and the Equation 2.

	N-emulsion	C-emulsion	A-emulsion
Coverage (prepared at 24 000 rpm)	77% ± 8%	60% ± 6%	90% ± 9%
Coverage (prepared at 6 500 rpm)	94% ± 9%	68% ± 7%	94% ± 9%

The MSD was not reached even for the highest concentrations of particles. When the MSD is reached, the calculated coverage drastically increases because the particles which are not adsorbed are taken in the balance. Such phenomenon was not observed. It has also been checked by light scattering measurements the absence of a population corresponding to free particles in suspension in the aqueous phase, meaning that the vast majority of them was adsorbed to the oil droplets.

The maximum stability corresponds to a maximum coverage. But it was expected that the higher the surface charge of the particles, the lower the droplet coverage because charged particles underwent strong electrostatic repulsions (33). Indeed, Horozov *et al*. observed that charged solid particles organized as a 2D colloidal crystal at the oil-water interface because of long range electrostatic repulsions between them. Such an observation was nevertheless restricted to highly hydrophobic silica particles with water/oil contact angle larger than 130° (34). In our case, C-emulsions would meet this expectation quite well as they exhibited the lowest coverage of 60% (Table 3). The A-emulsions had the highest coverage (~90%) although they had a similar surface charge. Intermediate coverage ~77% was obtained for N-emulsions. The contact angle between the polymer, water and oil was measured around 110° for all three types of polymers. For this contact angle, Horozov *et al.* observed both a random organization and 2-dimentionnal aggregation phenomena.

CLSFM pictures were taken to qualitatively confirm these trends. For each of the MTPs, isolated droplets were captured, and an enlargement was made to visualize the particles organization at the droplet surface (Figure 5). In all instances, CLSFM showed quite densely adsorbed particles arranged as a 2D coating. The pictures did not show aggregates of particles protruding in the direction normal to the surface. It appeared that all particles were in contact with oil, such that they were partially wet by oil and water. As an outcome, the particles were adsorbed on the droplets as a monolayer with high surface densities ranging between 60% and 90%. Two mechanisms are proposed to explain such results.

Firstly, concerning the difference of coverages between the three MTPs, a difference between anionic, neutral and cationic particles stands in their kinetics of adsorption at the oil-water interface. Indeed, it has been shown that the interface between pure oil and pure water is negatively charged because of the presence of adsorbed hydroxide ions (35). The electrostatic

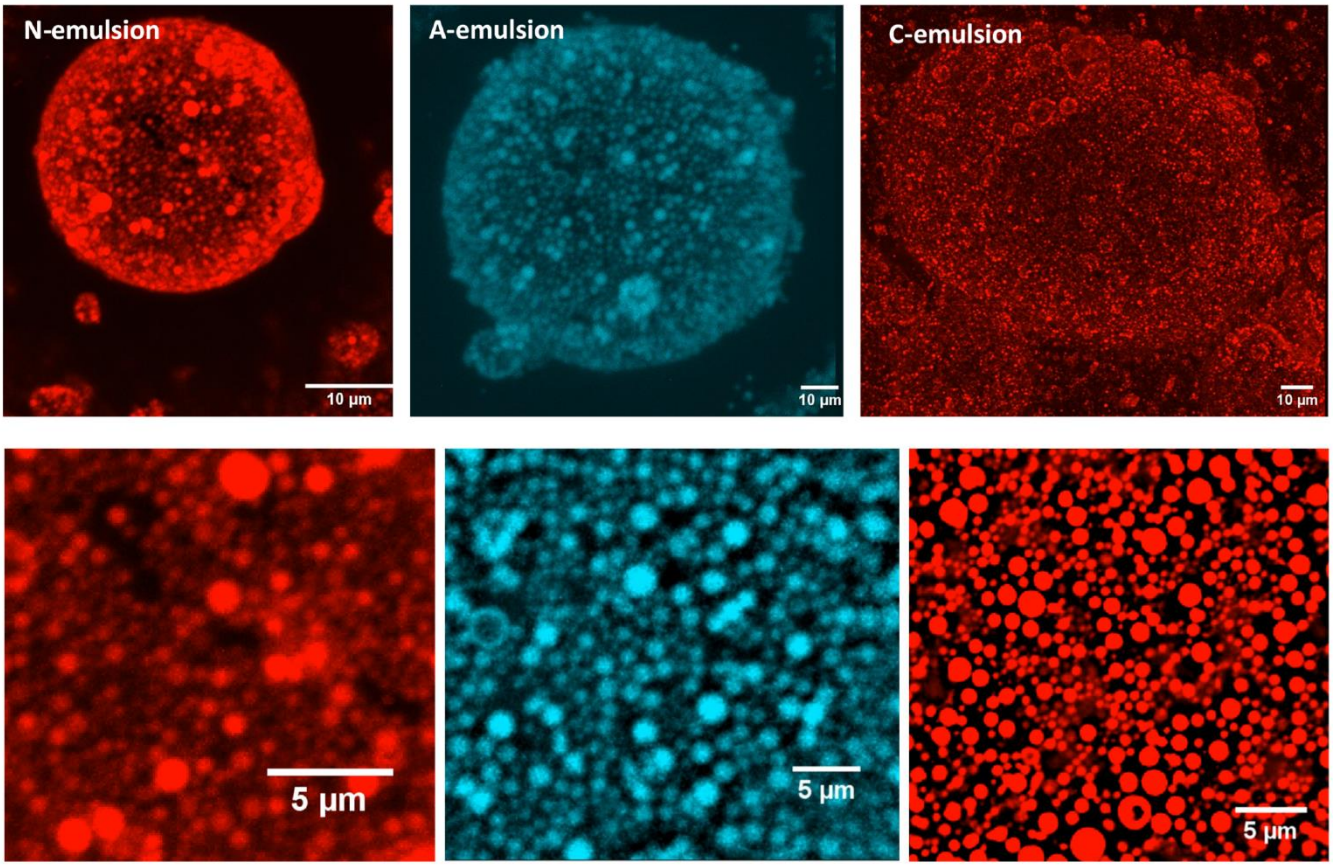

Figure 5. CLSFM pictures of the droplets from the different single particle type emulsions. From left to right, N-emulsion, A-emulsion and C-emulsion. The pictures on top show the 3D projection of the droplets and the bottom pictures are zooms at the surface of the droplets. An FFT filter was used to better visualize the particles at the surface.

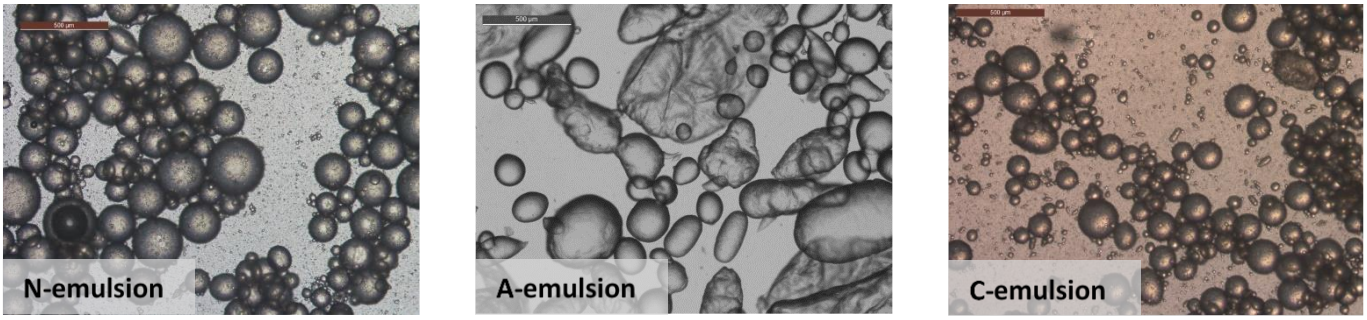

Figure 6. Optical microscope pictures of N-, A- and C-emulsions (from left to right). The concentration of particles was 21 mg of particles per cm^3 of oil. The scale bar is 500 µm.

barrier against adsorption could induce a slower adsorption of negatively charged particles compared to neutral ones, and a faster adsorption of positively charged ones. Such observations have already been reported in the literature. Larson-Smith *et al.* studied the adsorption of charged nanoparticles and noted that positively charged ones were especially attracted to the charged hexadecane/water interface (36). A recent example is given by the OCP double layer emulsions studied by Tao *et al.* (2) who observed that the positively charged particles adsorbed first at the interface. Fast adsorption leaves the particles at the position where they reached the surface, that is, in contact with the most external previously adsorbed particles. This quickly leads to a strong steric stabilization of the droplets. A slow adsorption of particles allows for their re-organization at the interface into a monolayer bringing a weaker steric stabilization. This phenomenon is similar to the 3D aggregation process where a fast diffusion-limited colloid aggregation (DLCA) yields aggregates of low density, whereas a reaction-limited colloid aggregation (RLCA) leads to denser aggregates (37,38). As the size of the droplets is linked to the competition between stabilization and back-coalescence, a strong stabilization of the interface would lead to less back-coalescence, then to smaller droplets, and thus to a lower coverage. Then, the kinetic of adsorption, rather than reaching a high final stability, would be the mechanism governing the droplets diameter. The influence of the kinetic of adsorption on the droplets diameters was already observed in the case of emulsions stabilized by differently shaped particles (29).

Secondly concerning the very high calculated droplet coverage in the A-emulsions, this observation could be linked to the instability of the droplets just after their fragmentation during the emulsification process. Indeed, it was noticed when measuring the droplets diameters, that many droplets in the A-emulsions were non-spherical contrary to N- and C-emulsions (Figure 6). The very high coverage (around 90%) calculated under the assumption of a spherical shape corresponds to what would be reached if the droplets did not deform (See SI4). According to Pawar *et al.* (39), non-spherical droplets with maximum coverage are due to the merging of two droplets having dense coverages, between 60% and 80% in their article. The strong anchoring of particles to the droplets surface prevent them for leaving the surface and a deformation into non-spherical shape of the droplets compensates the decrease of interfacial area due to coalescence. Indeed, there is no significant difference of particle density at the droplets surface in the CLSFM images of the three emulsions (Figure 5). An increase of interfacial area by 20% because of the deformation would reduce the surface density of particles from 90% down to 70%. Therefore, it is presumed that the emulsification process broke up oil droplets down to a size yielding a coverage around 60–80% like the other emulsions, and that an instability led to their partial coalescence and the deformation of oil droplets. As described before, that could result from the slow adsorption of a-PMMA. If the adsorption is slow compare to the back-coalescence, it is likely that droplets with high coverages would merge into non-spherical ones due to arrested coalescence. It is worth noting that arrested coalescence was observed in several other studies for coverage as high as 85% (40,41). The final A-emulsions were stable for several months however.

The first mechanism of a kinetically controlled phenomenon was checked by additional experiments with emulsions prepared using a stirring rate at 6 500 rpm instead of 24 000 rpm that would slow down the diffusion of particles to the droplets through the stagnant layer around them (42). The size of the droplets for emulsions made at 6 500 rpm for a same mass of particles introduced was significantly higher for N- and C-emulsions because the stirring rate was lower (Table 4). This was not the case for the A-emulsion because the droplet size was not controlled by the stirring rate, but by the limited coalescence leading to non-spherical droplets. The results of coverage for emulsions made at 6 500 rpm are presented in Table 3. They tend to confirm a kinetically controlled mechanism as the coverage increased significantly for C- and N-emulsions (*t*-test, $p < 0.05$).

Table 4. Comparison of the diameters of the droplets between emulsions made at 24 000 rpm and emulsions made at 6 500 rpm.

Emulsion type	Particle concentration ($mg \cdot cm^{-3}$ of oil)	Droplets diameter (µm)	
		24 000 rpm	6 500 rpm
N-	21	127 ± 11	143 ± 13
	34	71 ± 6	86 ±8
A-	21	148 ± 13	152 ± 14
	34	96 ± 9	87 ± 9
C-	21	137 ± 12	155 ± 14
	34	77 ± 7	100 ± 9

It is worth noting that N-emulsions made at 6 500 rp, had a coverage around 91%, corresponding to a hexagonal compact 2D organization. Nevertheless, at contrary to the A-emulsions, the droplets were spherical. Thus, that coverage did not result from the limited coalescence phenomenon (Figure 7).

DCPs: Emulsions made with differently charged particles.

i) Droplets size vs particle concentration for 50/50 w/w DCP. The results were similar to the previous ones using MTPs. The size of emulsions prepared with 50/50 w/w of three differently charged (A/N-, N/C-, A/C-emulsions) is presented in Figure 8 as a function of the inverse of the mass of particles. The size of the droplets varied linearly ($R^2 > 0.92$) with the mass concentration of particles in oil ranging from 8 up to 40 mg·cm^{-3} corresponding to median diameters between 60 µm and 405 µm. The A/C-emulsions droplets were bigger than other DCP-based emulsions. This is due to the fact that n-PMMA were smaller than a- and c-PMMA. A/N- and N/C-emulsions had similar droplets size. The differences are better discussed in term of coverage.

To get deeper insight into the impact of the composition of particles mixtures on the droplet coverage, DCP emulsions were prepared at 75/25 and 25/75 w/w. The results are given for each pair of particles in the next sections.

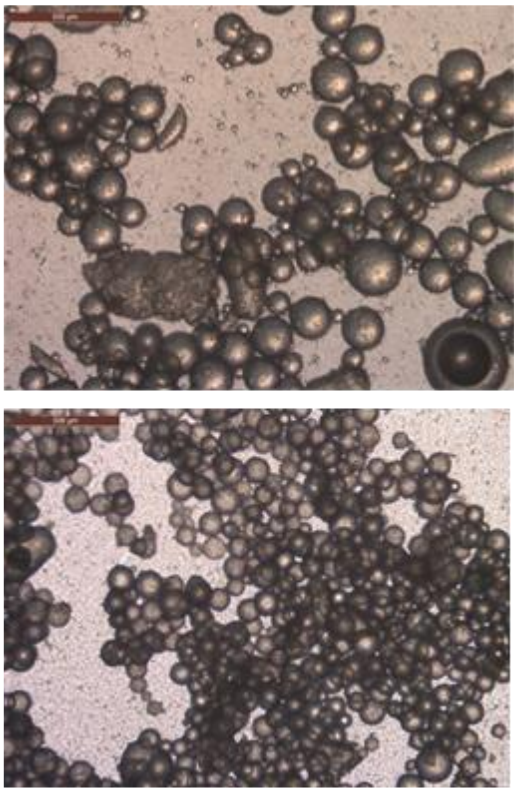

Figure 7. Optical microscope pictures of N-emulsions made at 6 500 rpm. The concentrations of particles were 21 mg of particles per cm^3 of oil (top) and 34 mg of particles per cm^3 of oil (bottom). The scale bar is 500 µm.

ii) DCP emulsions stabilized by mixed neutral and cationic particles. The coverages observed for these DCPs were equal to the mean coverage of N- and C-emulsions, weighted by the composition (between 77% and 60% at 24 000 rpm and between 94% and 68% at 6 500 rpm) (Figure 9). As previously noted, the coverage value is higher when the emulsion is made at 6 500 rpm. The kinetic explanation previously given still holds in the present case. A faster adsorption led to a lower coverage. To differentiate the particles when using a CLSFM, "blue" marked neutral particles were used in the binary mixture. Pictures of the emulsions taken by CLSFM showed that the droplets were covered by both mixed particles' types randomly distributed at the interface (Figure 10). The hypothesis stating that emulsion formation was limited by the particle adsorption kinetics could explain this observation. As n- and c-PMMA have few interactions, they should not affect the adsorption rate of

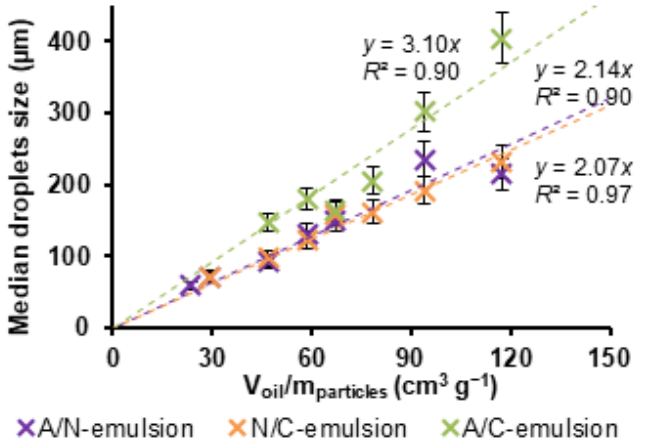

Figure 8. Median size of the droplets of the Pickering emulsions prepared with two different types of particles at 50/50 w/w as a function of the inverse concentration of particles. The volume of oil was kept constant and the mass of particles varied.

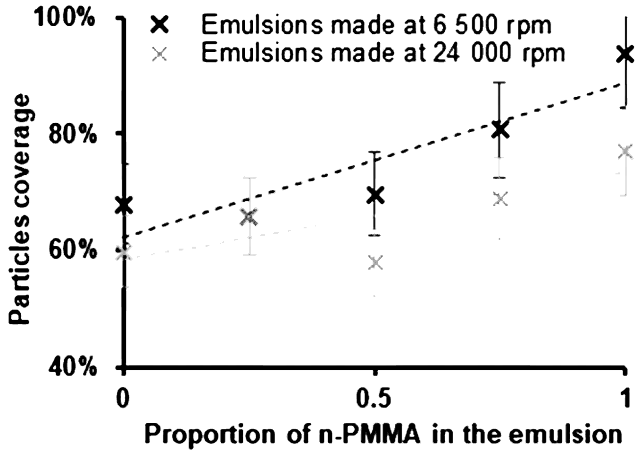

Figure 9. Coverages of the N/C-emulsions droplets as a function of the emulsion composition.

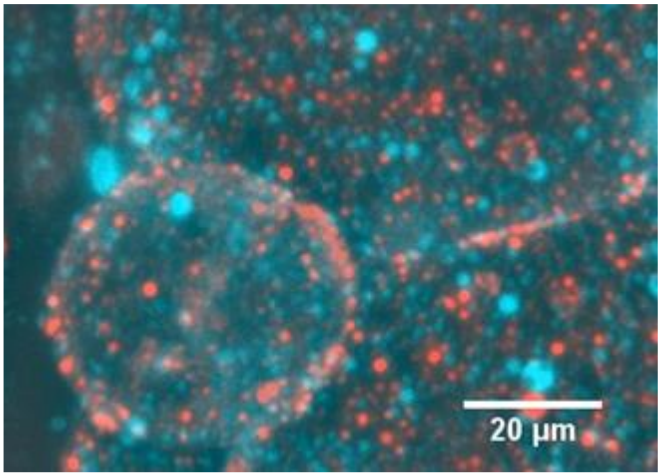

Figure 10. CLSFM image of N/C-emulsion made at 24 000 rpm. Neutral particles are in blue and cationic particles are in red. Results were similar for emulsions made at 6 500 rpm.

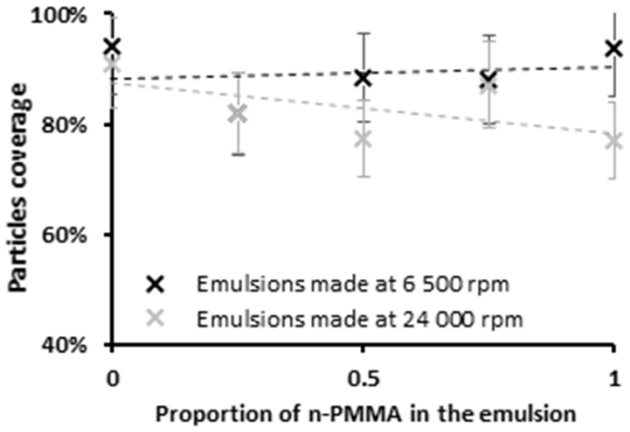

Figure 11. Coverage of the A/N-emulsions droplets as a function of the emulsion composition.

each other, and thus that the adsorption rate of the mixed particles is an average between both. It is worth noticing than no purple spot can be seen on this picture and the following ones. Purple spots would have been seen in case of a superimposition of two particles as shown in the simulation in Figure S5. This observation confirms the monolayer adsorption.

iii) DCP emulsions stabilized by neutral and anionic particles. At 24 000 rpm, the droplet coverage of DCP emulsions made of neutral and anionic particles varied between 77% and 90% with the particle composition (Figure 11). The trend is similar to the one observed for N/C-emulsions, the coverage obtained is the average of MTPs' ones weighted by the composition. Similarly to N/C-emulsions, interactions between a- and n-PMMA are weak, and thus the adsorption rate of the mixed particles is likely to be a weighted average. It is meant by weak interactions that no electrostatic interactions exist between both particles and that other interactions (van der Walls, hydrogen bonding,…) are considered negligible compared to the agitation.

At 6 500 rpm, these DCP emulsions had similar coverage around 90% which is the maximal reachable coverage. These values were also obtained for the emulsions stabilized by neutral or

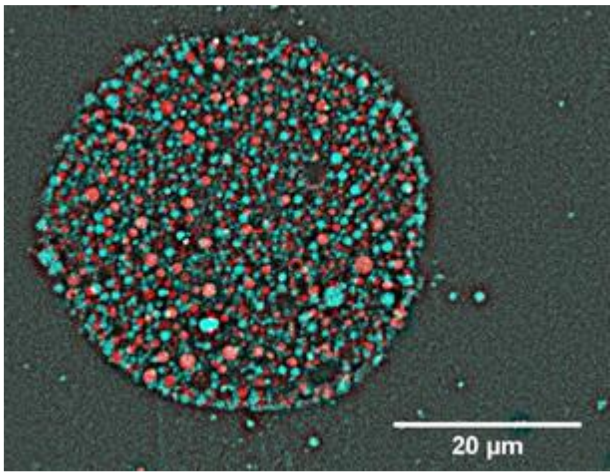

Figure 12. CLSFM image of A/N-emulsion made at 24 000 rpm. Neutral particles are in red and anionic particles are blue. Results were similar for emulsions made at 6 500 rpm.

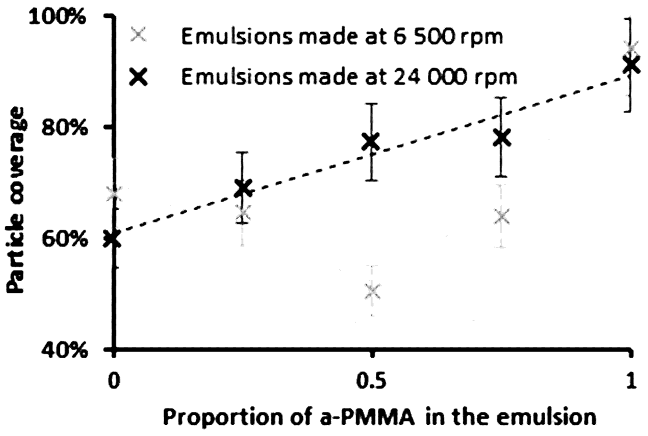

Figure 13. Coverage of the A/C-emulsion droplets as a function of the emulsion composition.

anionic particles (~94%, Table 3). Once again, their coverages corresponded to the weighted averages of the ones from mono-particles emulsions (Figure 11). As previously observed for DCP emulsions stabilized with cationic and neutral emulsions, confocal pictures show that the particles were randomly distributed and mixed at the surface of the droplets (Figure 12).

iv) OCP emulsions stabilized by cationic and anionic particles. The behavior of OCP emulsions prepared with mixtures of anionic and cationic particles was quite different. At 24 000 rpm, the droplet coverage varied as a weighted average from 60 up to 90% with the mass fraction of a-PMMA in the emulsion (Figure 13). As previously observed, the coverage corresponded to a weighted mean value obtained from the coverages of the corresponding MTPs. Both types of particles were also observed randomly distributed at the droplet surface (Figure 14). The particles behave as if there were no interactions between them. The sizes of the droplets made at 6 500 rpm was much lower for OCPs than for the MTPs. They were minimum for a 50/50 mixture. At 50/50 w/w ratio, the median droplet diameter of an

emulsion made with 21 mg of particles per cm^3 of oil fell from 147 µm at 24 000 rpm to 88 µm at 6 500 rpm (Table 5).

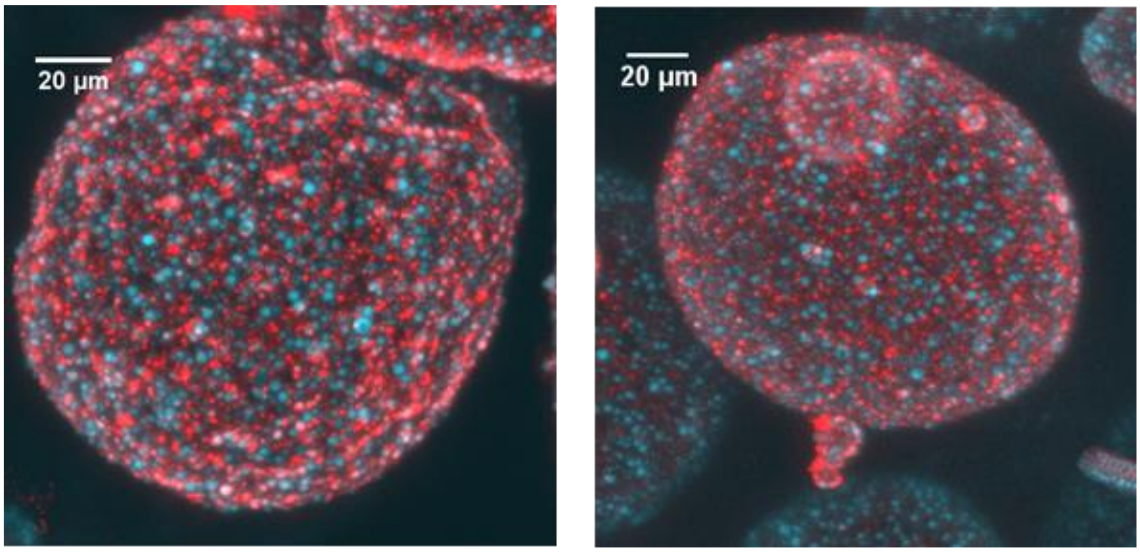

Figure 14. CLSFM images of A/C-emulsions made at 24 000 rpm (left) and at 6 500 rpm (right). Cationic particles are in red and anionic particles are in blue.

It was previously demonstrated that the coverage of a DCP emulsion varied as the weighted average of the corresponding MTPs. For the OCP emulsions made at 6 500 rpm, two regimes were observed. Indeed, the coverage varied between three values rather than two: the two MTPs ones (A- and C-emulsions) and an intermediate and lower value obtained with about 55% of anionic particles and 45% of cationic particles.

This third state could be due to the formation of neutral 3-dimentionnal aggregates of particles in the bulk. Indeed, the specific charges (charge/mass) of a-PMMA and c-PMMA were close (effective charge around 2.7 10^{15} per gram of particles in absolute value). Then, aggregates that they formed were likely to be composed of around 50/50 w/w of each particle. Nallamilli *et al.* (11) highlighted the fact that aggregation influences the adsorption mechanism of colloids, especially by lowering the charge of the particles. They prepared OCPs with latex particles that were more charged that the ones used in this article (ζ-potential =± 68 mV). These particles were supposed to be unable to adsorb at oil/water interface without being part of an aggregate due to the electrostatic repulsions of their image charge in oil. Then, Nallamilli *et al.* suggested that the presence of aggregates in the bulk could modify the adsorption at an interface. But the authors did not analyze whether the adsorbing particles were aggregated in the bulk. Neither had they shown an experimental evidence that the single particles did not adsorb. In the present study, the situation was different because the single particles did adsorb at the interface in MTPs.

Table 5. Droplet median sizes for different A/C-emulsions made at 24 000 rpm and 6 500 rpm (total concentration of particles in oil of 21 mg cm^{-3}).

Stirring	Droplets median diameter (µm)		
	A/C-emulsion: 25/75 w/w	A/C-emulsion: 50/50 w/w	A/C-emulsion: 75/25 w/w
24 000 rpm	139	147	138
6 500 rpm	128	88	113

The effect of electrostatic attraction between c-PMMA and a-PMMA on their adsorption rate was only observed when the stirring rate of the emulsification process was low (6 500 rpm). It was presumed that 3D aggregates were broken at the highest stirring rate (24 000 rpm). The influence of the stirring rate was investigated in a series of experiments where size measurements were made using a light scattering instrument. The mixing of particles was done in the beaker supplying the measurement cell of the light scattering instrument with a circulation of sample. The stirring rate varied from 500 rpm up to 3 500 rpm (the maximum available stirring rate) before being injected in the circuit. A linear relationship with very good correlation (R^2 > 0.99) was found between the inverse of the aggregates median diameter and the rotation speed of the mixer (Figure 15). According to an extrapolation to 6 500 rpm, aggregates should have a size of 2.50 µm, meaning that they should be composed of about 20 elementary particles. At 24 000 rpm, the size would correspond to only one elementary particle indicating that no aggregate is present in the aqueous dispersion under stirring.

According to one point of view, the presence of 3D aggregates in the bulk during the emulsification process may not explain the formation of smaller droplets at 6 500 rpm (Table 5). A slower agitation usually yields a higher coverage and leads to bigger droplets. Indeed, if 3D aggregates were adsorbing at the surface of the droplets, they would act as big and less numerous

particles ensuring a lower coverage, thus leading to bigger droplets. However, adsorption of an aggregate brings to the surface several primary particles at the same time. Considering an aggregate as a particle, according to the Stokes-Einstein law, its diffusivity is inversely proportional to its diameter whereas the number of primary particles in an aggregate increases steeper with respect to its diameter. It varies as the third power of its diameter for dense aggregates or to its diameter to the power the aggregate fractal dimension in case of loose aggregates.

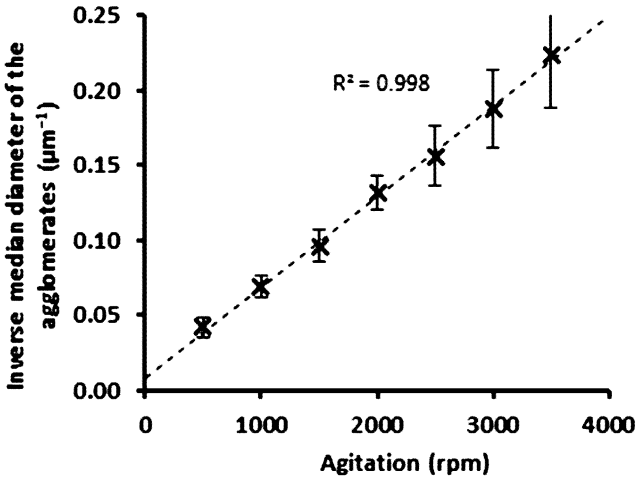

Figure 15. Size of the anionic/cationic (50/50 w/w) particle aggregates as a function of the stirring rate.

The balance is a faster adsorption in terms of primary particles. CLSFM did not detect any 3D aggregate at the surface of the droplets (Figure 14). Pictures better corresponded to a monolayer of particles. A re-organization of the adsorbed particles was possible once the 3D aggregates have been adsorbed because are not stuck together. They may roll on each other so that particles belonging to the part of the aggregates oriented towards the aqueous phase and that are not in contact with oil, finally can reach the oil-water interface and adsorb. Even if the adsorption of the 3D-agglomerates would be slow, the adsorption rate of the particles would significantly increase. Let us recall that the adsorption energy coming from partial wetting is very high. It is worth noting that once at the surface, the oppositely charged particles could form 2D aggregates.

3.2.3. Minimum size of the droplet. MSD was reached by preparing emulsions with a large concentration of particles in oil (212 mg cm^{-3}). The MSD corresponds to emulsions in which the maximum droplet coverage is reached without any particles present in the external phase. The presence of excess particles in suspension in the aqueous phase was assessed by light scattering measurements and allowed the determination of the MSD (18) (results not shown). MSD_d stands for dimensionless MSD; it is equal to MSD divided by the particle diameter. Indeed, as the particles size directly impact the size of the droplets, MSD_d was a more accurate parameter to compare sizes of different emulsions. Several repetitions of droplets sizes measurements were done and their precision was about 2 µm. Three categories of emulsions could be identified using the MSD_d values (Table 6). The A-, C-, A/C-emulsions whose MSD_d values were around 21. The N/C-, A/N-, and A/C(6 500 rpm)–emulsions whose MSD_d values were around 26, and the N-emulsion whose MSD_d was 62.

It was expected that charged particles would show a lower MSD_d. Indeed, as the charge is supposed to cause an electrostatic repulsion between the droplets, the back-coalescence is less likely to occur and then lower MSD can be reached. This argument can also be applied to N-emulsion as an explanation of its very high MSD_d.

N/C- and A/N-emulsions droplets were also charged, but 50% less than the ones from A- and C-emulsions. Then the repulsions between the droplets was lower, the back-coalescence effect was stronger, and their MSD_d was higher. Nevertheless, their MSD_d was half that of N-emulsions.

The results for both A/C-emulsions is more intriguing. As expected firstly, diminishing the stirring rate led to higher MSD. But even when the emulsion droplets were neutral, their MSD_d was similar to the ones of A- and C-emulsions. From MSD and coverage values obtained for the different emulsions, the theoretical maximum concentration of particles $c_{p,\max}$ that can be adsorbed to emulsion droplets was determined using:

$$c_{p,max} = \frac{d_p}{d_d}\, 4\rho * Coverage \qquad \text{(Eq. 3)}$$

The largest $c_{p,\max}$ was obtained for A- and A/C-emulsion (Table 6). It was lower one by 30% for the C-emulsion. Then, due to their lower MSD_d, A/N-, N/C- and A/C (6500)-emulsions had a $c_{p,\max}$ around 110 mg·cm^{-3} which was twice the value for the N-emulsion.

A high $c_{p,\max}$ is particularly interesting when the emulsion is used as a drug carrier system. Indeed, particles can contain active substances and a higher $c_{p,\max}$ allows for a larger loading inside the particles adsorbed on the emulsion droplets.

This last part highlights the interest in using DCPs when formulating Pickering emulsions. Indeed, anionic or cationic emulsions shows very low MSD_d. On the contrary, neutral emulsions have a high MSD_d, which could be limiting when trying to control some end-use properties (texture, density, …). This high MSD_d also limits the drug loading of the emulsion when the particles are used as delivery systems. Then, the use of DCPs allows to drastically reduce the MSD_d. The use of OCPs is also a way to obtain a neutral emulsion with a MSD_d similar to the charged ones.

Table 6. MSD and maximal particle concentration for different single type-particle-and DCP (50/50 w/w) emulsions prepared at 24 000 rpm (except the last one).

Emulsion	MSD (µm)	MSD_d = MSD / Particle diameter	$c_{p,max}$ (mg cm^{-3})
A-	17	23	195
N-	40	62	58
C-	20	21	134
A/C-	17	20	186
N/C-	19	24	110
A/N-	20	29	117
A/C- (6 500 rpm)	21	25	105

4. Conclusion

This article disclosed important properties of Pickering emulsions stabilized by Differently Charged Particles. DCP emulsions were prepared using binary mixtures of three types of particles (neutral, cationic and anionic). The charges of the particles have an impact on the coverage of the emulsion droplets by the solid particles. The more negatively charged a particle, the higher the droplet coverage. Such phenomenon was interpreted as a kinetically driven mechanism.

Both particle type and mixture composition influenced the coverage of the final emulsion droplets. Indeed, the coverage of DCP emulsions prepared with neutral particles varied linearly between those of the corresponding MTP emulsions. This average behaviour is due to low interactions between neutral particles and charged ones which result in an average adsorption rate. For OCP emulsions, evidence of an additional intermediate state was given; it was due to the formation of aggregates in the bulk. The size of the aggregates depended on the stirring rate and so did the coverage of OCP emulsions. By simply measuring the coverage and droplets size of the MTPs and of the intermediate state for OCPs, it is possible to predict the coverage and diameter of droplets stabilized with binary mixtures of particles.

Finally, DCP emulsions allowed to access lower minimum droplet size (MSD) and higher maximal concentration of particles than the corresponding MTPs. In particular when formulating emulsion with neutral droplets, the use of anionic and cationic particles led to a lower MSD. And, when using neutral particles, DCPs' formulation allow a higher particles concentration. More, OCP emulsions appeared to be a promising way to develop new drug delivery systems. The addition of a second type of particles is a way to tune the properties of Pickering emulsions, giving more freedom in term of designing emulsions.

Author Contributions

Mathis Benyaya: Conceptualization, Investigation, Methodology, Visualization, Writing - Original draft
Marie-Alexandrine Bolzinger: Conceptualization, Supervision
Yves Chevalier: Conceptualization, Supervision, Writing – Review and editing
Salomé Ensenat: Investigation
Claire Bordes: Conceptualization, Formal analysis, Supervision, Writing – Review and editing

Conflicts of interest

There are no conflicts to declare.

Acknowledgements

We are grateful to the Centre Technologique des Microstructures of the University of Lyon 1 (CTµ, http://microscopies.univ-lyon1.fr/) for their help on collecting the CLSFM images.

Notes and references

1 D. Gonzalez Ortiz, C. Pochat-Bohatier, J. Cambedouzou, M. Bechelany and P. Miele, *Engineering*, 2020, **6**, 468.
2 S. Tao, H. Jiang, R. Wang, C. Yang, Y. Li and T. Ngai, *Chem. Commun.*, 2020, **56**, 14011.
3 Y. Chevalier and M.-A. Bolzinger, *Colloids Surfaces A: Physicochem. Eng. Aspects*, 2013, **439**, 23.
4 J. Frelichowska, M.-A. Bolzinger, J.-P. Valour, H. Mouaziz, J. Pelletier and Y. Chevalier, *Int. J. Pharm.,* 2009, **368**, 7.
5 S. Simovic, N. Ghouchi-Eskandar and C. A. Prestidge, *J. Drug Deliv. Sci. Technol.*, 2011, **21**, 123.
6 C. Albert, M. Beladjine, N. Tsapis, E. Fattal, F. Agnely and N. Huang, *J. Control. Release*, 2019, **309**, 302.
7 C. Bordes, M.-A. Bolzinger, M. El Achak, F. Pirot, D. Arquier, G. Agusti and Y. Chevalier, *Int. J. Cosmetic Sci.*, 2021, **43**, 432.
8 M. Hristova, I. Lesov, S. Tcholakova, V. Goletto and N. Denkov, *Colloids Surfaces A: Physicochem. Eng. Aspects*, 2018, **552**, 142.
9 N. Madhavan, M. Mukherjee and M. G. Basavaraj, *Langmuir*, 2020, **36**, 11645.
10 T. Nallamilli, E. Mani and M. G. Basavaraj, *Langmuir*, 2014, **30**, 9336.
11 T. Nallamilli, B. P. Binks, E. Mani and M. G. Basavaraj, *Langmuir*, 2015, **31**, 11200.
12 M. Zembyla, A. Lazidis, B. S. Murray and A. Sarkar, *Langmuir*, 2019, **35**, 13078.
13 S. Tao, H. Jiang, S. Gong, S. Yin, Y. Li and T. Ngai, *Langmuir*, 2021, **37**, 8577.
14 S. Zhang, B. S. Murray, N. Suriyachay, M. Holmes, R. Ettelaie and A. Sarkar, *Langmuir*, 2021, **37**, 827.
15 F. Wu, J. Deng, L. Hu, Z. Zhang, H. Jiang, Y. Li, Z. Yi and T. Ngai, *Colloids Surfaces A: Physicochem. Eng. Aspects*, 2020, **602**, 125082.
16 R. van Hooghten, V. E. Blair, A. Vananroye, A. B. Schofield, J. Vermant and J. H. J. Thijssen, *Langmuir*, 2017, **33**, 4107.

17 L. G. Torres, R. Iturbe, M. J. Snowden, B. Z. Chowdhry and S. A. Leharne, *Colloids Surfaces A: Physicochem. Eng. Aspects*, 2007, **302**, 439.
18 J. Frelichowska, M.-A. Bolzinger and Y. Chevalier, *J. Colloid Interface Sci.*, 2010, **351**, 348.
19 M. P. Vasiliu, L. Sachelarie, L. E. Romila, E. Folescu, L. Atanase and A. Zaharia, *J. Biomim. Biomater. Biomed. Eng.*, 2016, **28**, 57.
20 E. Vargün, M. Sankir, B. Aran, N. D. Sankir and A. Usanmaz, *J. Macromol. Sci.*, Part A, 2010, **47**, 235.
21 S. Fleischmann and V. Percec, *J. Polym. Sci. A Polym. Chem.*, 2010, **48**, 4884.
22 C.-F. Lee, M.-L. Hsu, C.-H. Chu and T.-Y. Wu, *J. Polym. Sci. Part A: Polym. Chem.*, 2014, **52**, 3441.
23 P. van de Wetering, J.-Y. Cherng, H. Talsma, D. J. A. Crommelin and W. E. Hennink, *J. Control. Release*, 1998, **53**, 145.
24 M. Benyaya, M.-A. Bolzinger, Y. Chevalier and C. Bordes, *Polymer*, 2023, **272**, 125838.
25 H. Daoust and M. Rinfret, *J. Colloid Sci*., 1952, **7**, 11.
26 J. Brandrup, E. H. Immergut and E. A. Grulke, Eds., *Polymer Handbook*, Wiley, New York, 4th ed., 1999.
27 T. G. Fox and S. Loshaek, *J. Polym. Sci.*, 1955, **15**, 371.
28 B. P. Binks and S. O. Lumsdon, *Langmuir*, 2001, **17**, 4540.
29 M. Matos, A. Marefati, R. Bordes, G. Gutiérrez and M. Rayner, *Carbohydr. Polym.*, 2017, **169**, 127.
30 H. Ohshima, T. W. Healy and L. R. White, *J. Colloid Interface Sci.*, 1982, **90**, 17.
31 P. Sufi-Maragheh, N. Nikfarjam, Y. Deng and N. Taheri-Qazvini, *Colloids Surfaces B: Biointerfaces*, 2019, **181**, 244.
32 S. Arditty, C. P. Whitby, B. P. Binks, V. Schmitt and F. Leal-Calderon, *Eur. Phys. J. E*, 2003, **11**, 273.
33 F. Gautier, M. Destribats, R. Perrier-Cornet, J.-F. Dechézelles, J. Giermanska, V. Héroguez, S. Ravaine, F. Leal-Calderon and V. Schmitt, *Phys. Chem. Chem. Phys.*, 2007, **9**, 6455.
34 T. S. Horozov, R. Aveyard, J. H. Clint and B. P. Binks, *Langmuir*, 2003, **19**, 2822–2829.
35 K. G. Marinova, R. G. Alargova, N. D. Denkov, O. D. Velev, D. N. Petsev, I. B. Ivanov and R. P. Borwankar, *Langmuir*, 1996, **12**, 2045.
36 K. Larson-Smith, A. Jackson and D. C. Pozzo, *Langmuir*, 2012, **28**, 2493.
37 D. A. Weitz, J. S. Huang, M. Y. Lin and J. Sung, *Phys. Rev. Lett.*, 1985, **54**, 1416.
38 M. Y. Lin, H. M. Lindsay, D. A. Weitz, R. C. Ball, R. Klein and P. Meakin, *Nature*, 1989, **339**, 360.
39 A. B. Pawar, M. Caggioni, R. Ergun, R. W. Hartel and P. T. Spicer, *Soft Matter*, 2011, **7**, 7710.
40 G. Dockx, S. Geisel, D. G. Moore, E. Koos, A. R. Studart and J. Vermant, *Nat. Commun.*, 2018, **9**, 4763.
41 A. R. Studart, H. C. Shum and D. A. Weitz, *J. Phys. Chem. B*, 2009, **113**, 3914.
42 K. J. Mysels and H. L. Frisch, *J. Colloid Interface Sci.*, 1984, **99**, 136.

Supplementary Information

Pickering emulsions stabilized with Differently Charged Particles

Mathis Benyaya *, Marie-Alexandrine Bolzinger, Yves Chevalier, Salomé Ensenat, Claire Bordes *
Université de Lyon, Université Claude Bernard Lyon 1, CNRS UMR 5007, Laboratoire d'Automatique, de Génie des Procédés et de Génie Pharmaceutique (LAGEPP), 43 bd du 11 Novembre 1918, 69622 Villeurbanne, France

SI1. ^{1}H NMR spectra of the copolymers

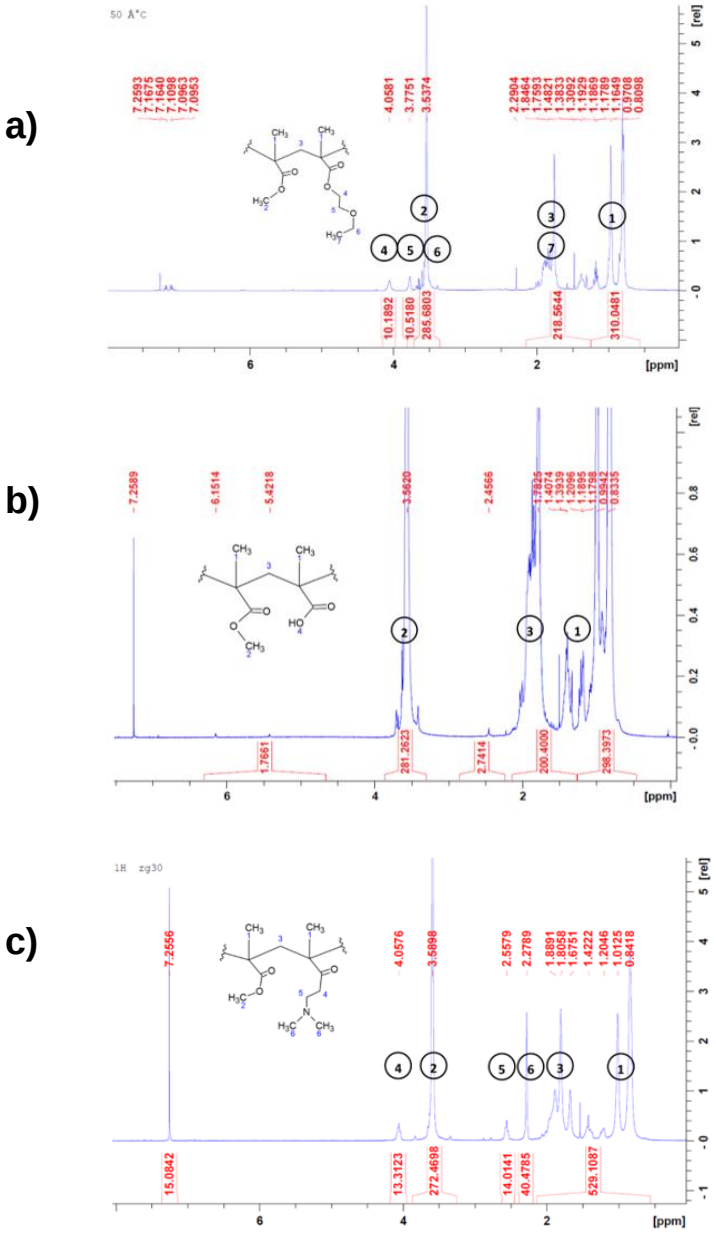

Figure S1. ^{1}H NMR spectra of N-PMMA (a), A-PMMA (b) and C-PMMA (c) copolymers. The peak at 7.25 ppm is that of the residual protons of the $CDCl_3$ solvent.

SI2. SEM pictures of the particles

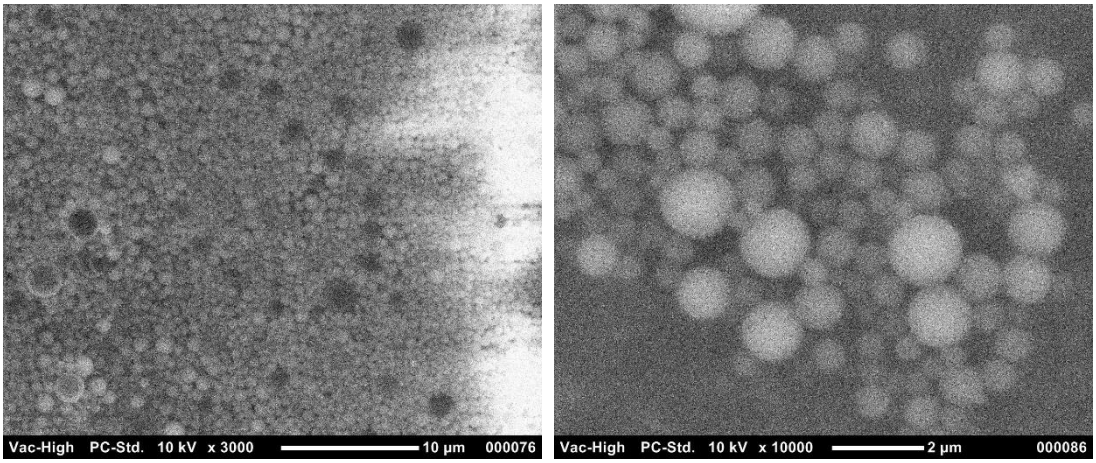

Figure S2. SEM images of a-PMMA at x3 000 (left) and x10 000 (right) magnification. Similar shapes were obtained for the other types of particles.

SI3. Aspect of the emulsions

Figure S3. Pickering emulsions made with 25 mg of particles per cm^3 of oil. From left to right N-, A-, C-, A/N-, N/C- and A/C-emulsions. The picture was taken 4 months after the preparation of emulsions. No release of free oil was observed on top of the emulsions.

SI4. Droplets diameters measurements for A-emulsions

To obtain the area of non-spherical droplets of various shapes, a mean (effective) diameter d_m was measured diagonally with respect to the directions of the long and short dimensions in the droplets.

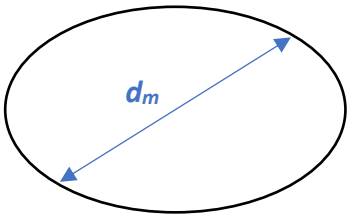

This diameter was then used as the apparent diameter of spherical droplets. So as to ensure that no systematic errors have been introduced by using d_m, the cross-section area of several non-spherical droplets from different emulsions were manually measured (using Image J) and compared with the spherical cross-section area calculated from d_m. The results are shown in the next tables for three A-emulsions. The absolute errors were always below 10% and the errors tend to compensate one another. Finally, the mean values of the cross-sectional areas calculated from d_m were close to the real ones (absolute errors below 5%), and less than the standard deviations of the diameters measurements for spherical droplets (9%).

Emulsion 1	**Measured "diameter" (µm)**	**Manually measured area (µm²)**	**Area calculated from the diameter (µm²)**	**Error (%)**
	132	14083	13682	−3%
	164	18372	21124	15%
	93	6879	6793	−1%
	105	8556	8659	1%
	131	13640	13478	−1%
	104	8756	8495	−3%
	125	12066	12272	2%
	151	18945	17908	−5%
Mean	***126***	***12662***	***12801***	***1%***

Emulsion 2	**Measured "diameter" (µm)**	**Manually measured area (µm²)**	**Area calculated from the diameter (µm²)**	**Error (%)**
	135	13521	14314	6%
	169	20330	22432	10%
	125	13483	12272	−9%
	155	15911	18869	19%
	149	17572	17437	−1%
	139	12845	15175	18%
	135	16333	14314	−12%
	133	13440	13893	3%
Mean	***143***	***15429***	***16088***	***4%***

Emulsion 3	**Measured "diameter" (µm)**	**Manually measured area (µm²)**	**Area calculated from the diameter (µm²)**	**Error (%)**
	152	16858	18146	8%
	132	14954	13685	−8%
	170	25100	22698	−10%
	152	21363	18146	−15%
	183	24397	26302	8%
	176	23 597	24328	3%
	160	20562	20106	−2%
	142	19292	15837	−18%
Mean	***158***	***20765***	***19906***	***−4%***

SI5. Simulation of a superimposition of particles in a CLSM picture

Two pictures of A-emulsion droplets colored in blue and in red were merged with Image J to simulate the superimposition of differently colored particles of a DCP emulsion caused by their adsorption as multilayers. The result of the stacking of both blue and red dots is a purple color of the droplets.

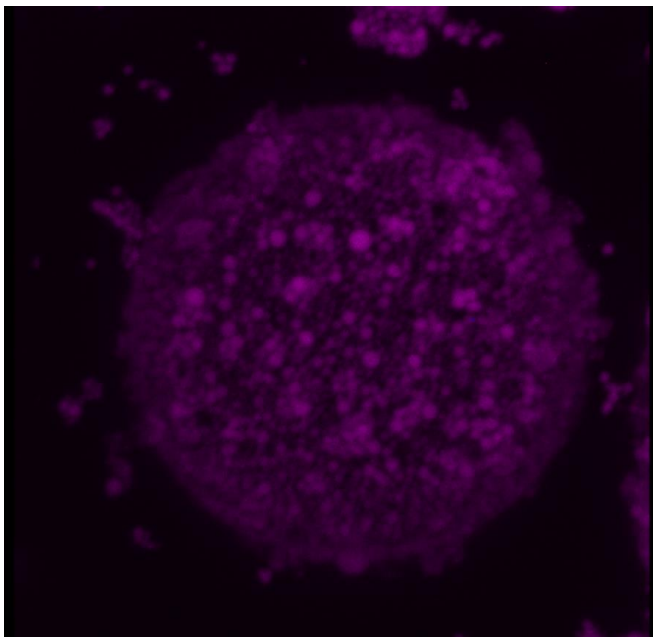

Figure S5. Merging of the same images colored in blue and in red. The superimposition of the particles with themselves appears as purple.